THE EUROPEAN
PHYSICAL JOURNAL B

X-ray photoelectron diffraction study of ultrathin PbTiO$_3$ films

L. Despont[1,a], C. Lichtensteiger[2], F. Clerc[1], M.G. Garnier[1], F.J. Garcia de Abajo[3], M.A. Van Hove[4], J.-M. Triscone[2], and P. Aebi[1]

[1] Institut de Physique, Université de Neuchâtel, Rue A.-L. Breguet 1, 2000 Neuchâtel, Switzerland
[2] DPMC, Université de Genève, 24 Quai Ernest-Ansermet, 1211 Genève, Switzerland
[3] Centro Mixto CSIC-UPV/EHU, 20080 San Sebastián, Spain
[4] Department of Physics and Materials Science, City University of Hong Kong, 83 Tat Chee Avenue, Kowloon, Hong Kong

Abstract. Full hemispherical X-ray photoelectron diffraction (XPD) experiments have been performed to investigate at the atomic level ultrathin epitaxial c-axis oriented PbTiO$_3$ (PTO) films grown on Nb-doped SrTiO$_3$ substrates. Comparison between experiment and theory allows us to identify a preferential ferroelectric polarization state in a 60 Å -thick PTO film. Multiple scattering theory based on a cluster-model [Phys. Rev. B **63**, 075404 (2001)] is used to simulate the experiments.

PACS. 77.80.-e Ferroelectricity and antiferroelectricity – 61.14.Qp X-ray photoelectron diffraction – 77.55.+f Dielectric thin films

Introduction

Ferroelectric oxides display a variety of interesting physical properties including piezoelectricity, pyroelectricity, and a non-volatile switchable electric polarization. This functionality makes them attractive candidates for numerous applications such as actuators, high frequency filters, infrared detectors, or high density non-volatile memories [1–3].

Recently, progress on the material side and new techniques have allowed ferroelectricity to be studied at nanoscale [4]. In particular, scanning probe microscopy has emerged as one interesting technique allowing local manipulations of domain structure in thin films and studies of ferroelectricity on nanometer scales [3,5,6]. Combining this technique with epitaxial Pb(Zr$_0$.2Ti$_0$.8)O$_3$ thin films, ferroelectricity was demonstrated down to 40 Å [5]. X-ray synchrotron was also used to study epitaxial PbTiO$_3$ thin films grown on insulating SrTiO$_3$ substrates and revealed periodic 180° stripe domains in films from 420 down to 12 Å thickness [7,8]. Very recently, a synchrotron X-ray micro-diffraction technique was developed to probe domain growth and switching in ferroelectric devices with submicrometer spatial resolution [9].

All the techniques described above are probing an average (throughout the depth of the films) response of the material. To get a more detailed microscopic information on ferroelectricity and to be able to directly probe the ferroelectric polar distortion, an atomic scale sensitive technique is needed. In this paper we show that X-ray photoelectron diffraction (XPD), already known as an important tool for crystal structure analysis might be a possible route to address the problem of ferroelectricity in ultrathin films. In particular, this technique is applied to PbTiO$_3$ (PTO), a ferroelectric perovskite with a tetragonal structure below the critical temperature T_c, characterized by two oppositely polarized ground states along the (polar) tetragonal c-axis [10–12]. These two "up" and "down" equivalent and electrically switchable states are characterized by the corresponding displacements of the Ti and O atoms in the unit cell delimited with Pb atoms, see Figure 1. For the data analysis and simulation of the experiment, the cluster-model approach of the EDAC code [13] is used.

Experimental and computational details

Here we study epitaxial c-axis oriented PbTiO$_3$ perovskite films grown using off-axis magnetron sputtering onto metallic (001) Nb-SrTiO$_3$ substrates. Topographic measurements using atomic force microscopy showed that these films are essentially atomically smooth. X-ray diffraction measurements allowed us to precisely determine the thickness of the films and the c-axis lattice parameter value, and to confirm epitaxial growth [14,15].

The samples were exposed to air during transfer from the growth chamber to the XPD experiment. No surface cleaning procedure was applied, and the measurements were performed at room temperature. Despite the
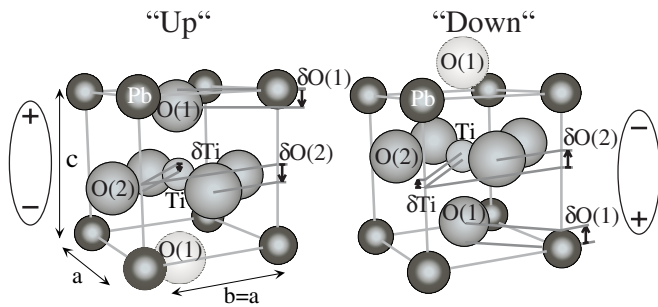
[a] e-mail: Laurent.Despont@Unine.ch

Fig. 1. Tetragonal PTO unit cell with the ferroelectric bulk lattice parameters $a = b = 3.902$ Å and $c = 4.156$ Å. The displacements, in fractional units, from cubic phase sites are $\delta Ti = 0.0377$ for titanium, $\delta O(1) = 0.1118$ for the first oxygen type (alternating along the c axis with the titanium) and $\delta O(2) = 0.1174$ for the second oxygen type (in the vertical Pb plane) [11]. The electric dipoles resulting from the ionic displacements are schematically shown.

Fig. 2. (a) XPS spectrum for PTO (60 Å thick film), obtained with MgKα radiation. O 1s (I) is the emission from the contamination layer while O 1s (II) has its origin within the PTO.

presence of surface contamination, we obtain well-defined diffraction patterns. Via X-ray photoelectron spectroscopy (XPS), Figure 2, we detect small amounts of C. In addition, the O 1s emission line is doubled due to oxygen atoms in chemically different environments (see inset of Fig. 2). One emission line has its origin from O within the PTO and the other from contaminants at the surface. The distinction is possible since the XPD pattern of the O 1s emission from the contamination layer, as well as from the C 1s emission does not show anisotropy whereas it does for O 1s emission from oxygen within the PTO. This also demonstrates that the contamination layer is disordered. The shift between both O lines is roughly 3 eV and allows a clear separation of the PTO oxygen from the one at the surface. The photoelectrons emitted from O contained in the substrate can not be detected as the thickness of the measured film, 60 Å is larger than their inelastic mean free path. that the polarization determination by selecting the O emission signal is limited to film thicknesses down to approximately 20 Å due to the presence of O in the substrate (also for the Ti emission). This limitation is also a function of the photoelectron kinetic energy which defines the distance after which the signal becomes negligibly small depending on the inelastic mean free path.

The XPD measurements were done in a modified Vacuum Generators ESCALAB Mk II X-ray photoelectron spectrometer equipped with a fixed hemispherical electron energy analyzer, and a three-channeltron detection system, operated with a base pressure in the lower 10^{-11} mbar region. X-ray photons are provided with a MgKα (hν = 1253.6 eV) and SiKα (hν = 1740 eV) twin anode. The samples are fixed on a computer-controled two-axis goniometer capable of scanning the emission angle over the full hemisphere above the surface [16,17].

A 2π emission-angle intensity scan of a given X-ray photoemission line permits the determination of the local geometry around the selected atom [18–21]. The angular dependence of the collected electron intensity originates from the interference of th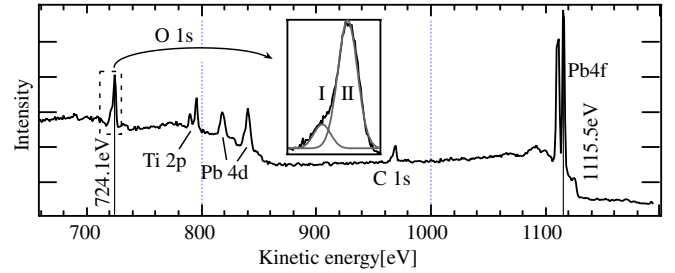e directly emitted photoelectron wave and the scattered electron waves. XPD being sensitive at an atomic scale, [22,23] it can be used to analyze crystal structures down to the monolayer and, in particular, to study ultrathin films of PTO. The knowledge of the crystal structure, then, allows us to discriminate between paraelectric and ferroelectric states.

The analysis of diffraction patterns is facilitated due to the so-called "forward focusing" effect occurring if the photoemitted electron has a kinetic energy above approximately 0.5 keV. Single scattering model calculations predict strong enhancement of the emission intensity in direction of near neighbours and more generally along densely packed rows of atoms which correspond to low-index crystallographic directions [24]. When compared to experimental results, the "forward focusing" intensity is overemphasized in single scattering calculations. This implies the necessity to use multiple scattering calculations (MSC). Furthermore, in the above-mentioned energy range the photoelectron inelastic mean free path (λ) is large. Thus the number of elastic scattering events is also large and therefore the use of MSC calculations becomes essential. In fact, scattering at the first few atoms along a row of atoms focuses the emission in the emitter-scatterer direction. Then, subsequent atoms tend to defocus the signal [25]. The defocusing is linked to the development of the conventional Kikuchi bands which become more intense when the forward-scattering peak intensity diminishes [25,26]. Therefore, MSC provides a solution to increase the accuracy in peak and band intensities as well as in structural details.

To simulate the XPD experiment, we use the cluster-model approach of the EDAC code [13] based on the muffin-tin potential approximation [27]. We employ the Haydock recursion method to calculate an iterative solution of the MSC series [13]. The chosen atomic positions in the clusters are taken from the bulk structure in reference [11]. The computation time needed to determine the scattered wave function is proportional to $nN^2(l_{max}+1)^3$, where n is the scattering order, N the number of atoms used in the cluster and l_{max} the maximum angular momentum quantum number. This last parameter permits an approximation of the outgoing photoelectron wave function using a combination of l_{max} spherical harmonics. The number of spherical harmonics is approximately given by $l_{max} \approx kr_{mt}$ [27] where k is the photoelectron momentum
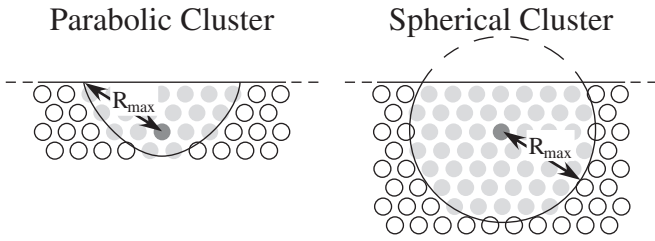
Parabolic Cluster   ## Spherical Cluster

Fig. 3. Two different cluster shapes with the scattering volumes defined by R_{max}. The light and dark gray disks correspond to scatterers and to the emitter, respectively.

and r_{mt} the muffin-tin radius. By assuming an average nearest-neighbor distance and selecting a photoelectron kinetic energy E_{kin}, we can roughly deduce the l_{max} parameter.

The number N of scattering atoms in the cluster is defined using the parameter R_{max}. In Figure 3 we show how R_{max} defines the scattering volume using the emitter, in the first case, as the focus of a parabola or, in the second case, as a sphere centre. Sufficiently large R_{max} have been used in the calculations to insure the convergence on the cluster size. To increase the contribution of scattering on atoms between the emitters and the surface, the parabolic shape is selected in the present study. In our case, the scattering volume contains approximately 150–250 atoms (R_{max} = 16–22 Å). We can deduce the electron inelastic mean free path λ by taking into account the universal relationship between energy and inelastic mean free path [28,29]. For each layer located within λ from the surface we take one of every inequivalent atom as emitter. For PTO, with $\lambda = 10$ Å for O 1s ($E_{kin} = 724.1$ eV, MgKα), seven (for the "up" state) and eight ("down" state) emitters are chosen over three unit cells while, with $\lambda = 17$ Å for Pb $4f_{7/2}$ photoelectrons ($E_{kin} = 1115.5$ eV, MgKα), five emitters (for "up" and "down" states) are selected over five unit cells.

The introduction of an inner potential V_0 permits to consider refraction effects of the photoelectron wave at the surface-potential step. A value of 10.5 eV is chosen [30]. Thermal vibrations are introduced by means of a Debye temperature (θ_D), and the θ_D have been introduced separately for each type of atom. We have taken values of $\theta_D = 105$ K, 420 K and 80 K for Pb, Ti and O atoms respectively [31]. The calculations were performed for a temperature $T = 300$ K.

Two different surface terminations are possible, but using XPD it is not possible to extract the surface termination in the case of PTO films. The reason is that in this system the contribution due to scattering of electrons from deeper layers at the top most layer is negligible compared to the direct emission from deeper layers. This behaviour originates from the small distance between the strong-scatterer layers (containing Pb). However, the calculations are performed with a Pb-O terminated surface. Indeed, Meyer et al. [32] suggest that only the Pb-O surface termination is thermodynamically stable in PTO.

Results and discussion

Analysis of the XPS spectrum presented in Figure 2 shows that the most intense signals come from the core levels of Pb and O. The signal for Ti emission is smaller. In addition, for both, the "up" and "down"-states, the displacement of the Pb atoms relative to the Ti atoms is smaller than the displacement of Pb atoms relative to the O atoms[11]. This signifies that the difference between the "up"- and the "down"-state "forward focusing" peak positions is smaller for the Ti emission than for the O emission. Moreover the polarization signature is located in the (110)-plane if Ti emitters are selected. This means that the Ti-Pb distance is larger than the O-Pb distance (in the (100)-plane), suggesting a smaller "forward focusing" peak intensity (exponential signal decrease along the photoelectron path due to the inelastic mean free path). Therefore, in the following we chose to analyze in details the Pb and O XPD patterns.

In Figure 4a the major low-index directions and crystal planes of the perovskite structure are plotted in stereographic projection. Calculated diffractograms for the Pb $4f_{7/2}$ core level are displayed in Figures 4b and 4c for the "up" and the "down" state cases, respectively, according to the structure of reference [11]. The experimental diffractogram for a 60 Å thick film is displayed in Figure 4d. All the diffractograms are plotted in stereographic projection. A background has been subtracted to all experimental data in the following manner: the total intensity was recorded at the kinetic energy corresponding to the maximum of the relevant peak (I_{peak}) and at its high-energy footpoint (I_{high}). The background-corrected intensity was then calculated by subtracting I_{high} from I_{peak}. The patterns have been azimuthally averaged exploiting the fourfold symmetry of the PTO and normalized to a smooth polar angle dependent background. As the calculations do not contain the secondary electron background, only the final normalization has been applied to the simulations.

The main "forward focusing" peaks, labelled A_1 ($\langle 111 \rangle$ directions), B_1 ($\langle 101 \rangle$ directions) and C_1 (normal emission, [001]) are at the same positions for both the simulations and the experiment, with similar intensities and widths. These peaks correspond to scattering by Pb atoms. The intensity modulations D_1 (between [001] and $\langle 101 \rangle$ directions), E_1 (between [001] and $\langle 111 \rangle$ directions) and F_1 (between $\langle 101 \rangle$ and $\langle 100 \rangle$ directions) have also the same behaviour for "up", "down" and the experiment. The intensity enhancements, G_1, on the {101} Kikuchi bands, near $\langle 121 \rangle$ directions are also comparable for the three different diffractograms. This is also true for the H_1 modulations. Polar cuts at $\phi = 0°$ are performed from the normal emission direction up to $\theta = 78°$ polar angle, in Figure 4e. The differences between both simulations are not large enough to distinguish between both polarization states.

Therefore, at this point, it is not possible to differentiate between the two different polarization states. The diffractograms are completely dominated by the scattering on the heavy Pb atoms. This is due to the larger Pb scattering cross section compared to Ti or O. As Pb is the
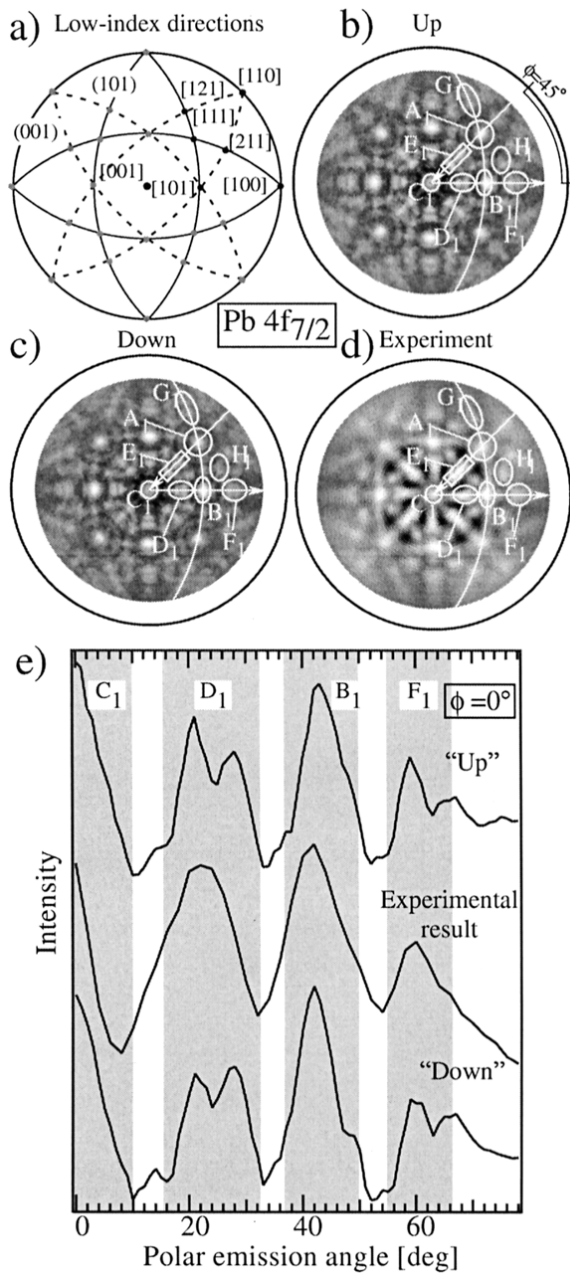
Fig. 4. MgKα excited Pb $4f_{7/2}$ photoelectrons at $E_{kin} = 1115.5$ eV. (a) Stereographic projection of major directions (dots) and low-index planes (continuous lines correspond to dominant high-density planes {101}, dashed lines correspond to minor high-density planes {$\bar{1}11$}). Simulated diffractograms for PTO (b) "up" and (c) "down" cases. (d) Experimental result for a c-axis oriented PTO 60 Å-thin film. (e) Polar cuts at $\phi = 0°$ for the two simulated states and the experimental case.

main scatterer in this material, the attention has to be focused on the Pb atom displacement relative to others kinds of atoms. By selecting O atoms as emitters, therefore, we change the reference system from which the photoelectrons are ejected. Instead of looking at the displacement of the light atom sublattice relative to Pb, we expect

to see the corresponding shifts of Ti and Pb atoms relative to O atoms.

The results displayed in Figure 5 show diffractograms obtained with the O 1s core level ($E_{kin} = 724.1$ eV). In Figure 5a we see the major low-index crystallographic directions and dominant high-density planes. In Figures 5b and 5c, we show the calculated diffractograms for PTO "up" and "down" state structures. Figure 5d displays the experimental result for the 60 Å thin film. To bring into evidence the region of large differences between the two different structures, polar cuts are presented at $\phi = 0°$ starting at normal emission [001] up to $\theta = 78°$ polar angle, plotted together with the experimental result along the same direction. The main difference comes from the scattering of O 1s photoelectrons on nearest neighbor Pb atoms (label A in Fig. 5), as expected from the previous result obtained with Pb emission. Near $\langle 101 \rangle$ directions we observe easily the corresponding principal "forward focusing" direction which appears to be the same in Figures 5b and d, namely for the "up" state structure.

In the Pb emission case, the dominant Kikuchi bands are the {101} and the main "forward focusing" peaks (label A_1 and B_1) are aligned on these bands, while for O emission the dominant Kikuchi bands are the {$\bar{1}11$} and the main peaks (label A) are shifted from the aligned position. This behaviour indicates that, in the first case, the dominant high-density planes are constituted by Pb atoms, and trivially, the peaks representing the scattering by Pb are along the bands. In the O emitter case, the diffraction on the crystal planes formed by O atoms is dominant. Then the main "forward focusing", O-Pb directions, are not aligned anymore with the bands. This behaviour is well observed where, for the "up" structure simulation and the experimental result (Figs. 5b and d), the peaks (label A) are inside the Kikuchi bands delimited zone, while they are outside of the same region for the "down" structure simulation (Fig. 5c). The information extracted from this region of the diffractogram is strongly influenced by the small distance between emitters and scatterers.

Furthermore we observe intensity enhancements (B) on {$\bar{1}11$} Kikuchi bands. The length and the width of this modulation agrees well between the experiment and the "up" state calculation. Similar features (C) appear close to $\langle 211 \rangle$ directions, but differences between "up" and "down" in this case are not significant enough to identify the different states. The center peaks (label D) originate from the scattering by O atoms, just above the selected emitters. As this configuration is exactly the same for "up" and "down" states, no information about the structure differences is revealed. The origin of the peak (label E), between [001] and the $\langle 101 \rangle$ directions, could not be extracted in a direct way and thus is linked to multiple scattering effects. As displayed in Figure 5e, this peak is not exactly reproduced in the "up" structure case but shows more similarity with the experimental result than in the "down" case, where there is a lack of intensity in the concerned region.

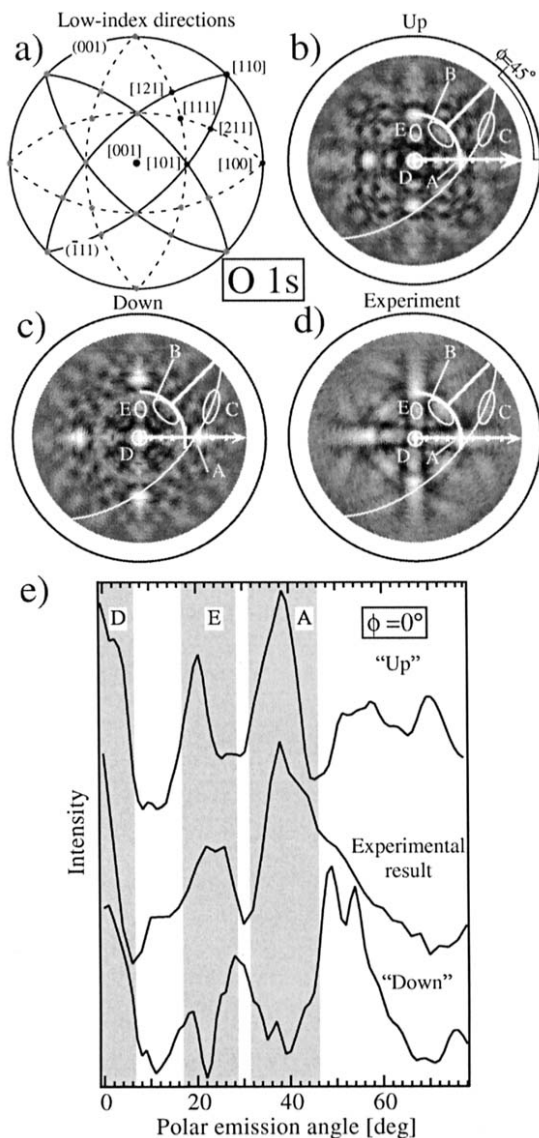As seen from Figure 5, the agreement of the calculation with experiment is good but not perfect. The reason

Fig. 5. MgKα excited O 1s photoelectrons at $E_{kin} = 724.1$ eV. (a) Stereographic projection of major directions (dots) and low-index planes (continuous lines correspond to dominant high-density planes $\{\bar{1}11\}$, dashed lines correspond to minor high-density planes $\{101\}$). (b) Simulated diffractogram for PTO "up" state plotted in stereographic projection. (c) The same calculation as in (b) but for the "down" state. (d) Experimental result for a c-axis oriented PTO 60 Å thin film. (e) Polar cuts at $\phi = 0°$ for the two simulated states and the experimental case.

may be found in the fact that we use structural parameters taken from the bulk [11]. In reality, surface relaxation may take place and a detailed optimization and a R-factor analysis of structural parameters will be required. Furthermore, PTO contains three highly different atomic types and the exact relative scattering strength and vibration parameters are difficult to determine. Correct relative scattering strengths are necessary to obtain accordance on relative intensities of interference features.

The intention here is to establish the basic principle for the use of XPD to investigate ultrathin ferroelectric films. We are able to make a clear distinction between the "up" and "down" state for a bulk-terminated surface, and subsequently we are able to characterize the sample as "up" polarized, according to angular positions, e.g. features A-E in Figure 5. In particular, the O-Pb first order near neighbour "forward focusing" direction (feature A) is practically given by geometrical consideration. Since Pb is the dominant scatterer (cf. Fig. 4, results for the Pb emission), the analysis concerning the large difference coming from peak A is therefore giving very robust information.

Conclusion

Calculations taking into account multiple scattering prove to be necessary to accurately simulate XPD diffractograms. Diffraction patterns are dominated by the "forward focusing" peaks along low-index crystallographic directions. Kikuchi bands appear with the same width and intensity as in the experiment. Regarding PTO, differences between "up" and "down" simulations are sufficiently large to be distinguishable when selecting the O 1s core level. Globally the agreement between experiment and calculation is good and allows us to identify our 60 Å film as "up" polarized.

References

1. T. Tybell, C.H. Ahn, J.-M. Triscone, Appl. Phys. Lett. **72**, 1454 (1998)
2. J.F. Scott, C.A.P. de Araujo, Science **246**, 1400 (1989)
3. P. Paruch, T. Tybell, J.-M. Triscone, Appl. Phys. Lett. **79**, 530 (2001)
4. C.H. Ahn, K. Rabe, J.-M. Triscone, Science **303**, 488 (2004)
5. T. Tybell, C.H. Ahn, J.-M. Triscone, Appl. Phys. Lett. **75**, 856 (1999)
6. P. Paruch, T. Giamarchi, J.-M. Triscone, Phys. Rev. Lett. **94**, 197601 (2005)
7. S.K. Streiffer, J.A. Eastman, D.D. Fong, C. Thompson, A. Munkholm, M.V. Ramana Murty, O. Auciello, G.R. Bai, G.B. Stephenson, Phys. Rev. Lett. **89**, 067601 (2002)
8. D.D. Fong, G.B. Stephenson, S.K. Streiffer, J.A. Eastman, O. Auciello, P.H. Fuoss, C. Thompson, Science **304**, 1650 (2004)
9. Dal-Hyun D. Paul, G. Evans, E.D. Isaacs, D. Min Kim, C. Beom Eom, E.M. Dufresne, Nature Materials **3**, 365 (2004)

10. T. Tybell, P. Paruch, T. Giamarchi, J.-M. Triscone, Phys. Rev. Lett. **89**, 097601–1–4 (2002)
11. R.J. Nelmes, W.F. Kuhs, Solid State Commun. **54**, 721 (1985)
12. F. Jona, G. Shirane, *Ferroelectrics Crystals* (Dover Publication, New York, 1997)
13. F.J. Garcia de Abajo, M.A. Van Hove, C.S. Fadley, Phys. Rev. B **63**, 075404–1–16 (2001)
14. C. Lichtensteiger, J.-M. Triscone, J. Junquera, P. Ghosez, Phys. Rev. Lett. **94**, 047603 (2005)
15. C. Lichtensteiger, J.-M. Triscone, Int. Ferroelectrics **61**, 143 (2004)
16. J. Osterwalder, T. Greber, A. Stuck, L. Schlapbach, Phys. Rev. B **44**, 13764 (1991)
17. D. Naumović, A. Stuck, T. Greber, J. Osterwalder, L. Schlapbach, Phys. Rev. B **47**, 7462 (1993)
18. R. Fasel, P. Aebi, J. Osterwalder, L. Schlapbach, Surf. Sci. **331**–**333**, 80 (1995)
19. J. Osterwalder, P. Aebi, R. Fasel, D. Naumović, P. Schwaller, T. Kreutz, L. Schlapbach, T. Abukawa, S. Kono, Surf. Sci. **331**–**333**, 1002 (1995)
20. D. Naumović, J. Osterwalder, A. Stuck, P. Aebi, L. Schlapbach, Surf. Sci. **287**–**288**, 950 (1993)
21. T. Greber, J. Osterwalder, D. Naumović, A. Stuck, S. Hüfner, L. Schlapbach, Phys. Rev. Lett. **69**, 1947 (1992)
22. R. Fasel, P. Aebi, R.G. Agostino, D. Naumović, J. Osterwalder, A. Santaniello, L. Schlapbach, Phys. Rev. Lett. **76**, 4733 (1996)
23. P. Aebi, R. Fasel, D. Naumović, J. Hayoz, T. Pillo, M. Bovet, R.G. Agostino, L. Patthey, L. Schlapbach, F.P. Gil, H. Berger, T. Kreutz, J. Osterwalder, Surf. Sci. **402**, 614 (1998)
24. C.S. Fadley, *Synchrotron Radiation Research: Advances in Surface Science* (Plenum, New York, 1990)
25. W.F. Egelhoff Jr., Critical Reviews in Solid State and Materials Sciences **16**, 213 (1990)
26. H.A. Aebischer, T. Greber, J. Osterwalder, A.P. Kaduwela, D.J. Friedman, G.S. Herman, C.S. Fadley, Surf. Sci. **239**, 261 (1990)
27. J.B. Pendry, *Low Energy Electron Diffraction* (Acamedic Press, London, 1974)
28. R.E. Ballard, J. Electron Spectrosc. Relat. Phenom. **25**, 75 (1982)
29. M.P. Seah, W.A. Dench, Surf. Interface Anal. **1**, 2 (1979)
30. At high electron kinetic energies, the effect of refraction (or V_0) is not very important
31. From the *Integral Scientist Periodic Table of the Elements (ISPT)*, available on `http://www.qivx.com`
32. B. Meyer, J. Padilla, D. Vanderbilt, Faraday Discuss. **114**, 395 (1999)